

1

2

3

4 **Main Manuscript for**

5 **SLC35G3 is a UDP-N-acetylglucosamine transporter for sperm glycoprotein formation and**
6 **underpins male fertility in mice**

7 **Authors:**

8 Daisuke Mashiko^{1,2}, Shingo Tonai¹, Haruhiko Miyata¹, Martin M. Matzuk^{3,4}, and

9 *Masahito Ikawa^{1, 2, 5, 6,7}

10

11 **Affiliation:**

- 12 1. Department of Experimental Genome Research, Research Institute for
13 Microbial Diseases, Osaka University, Suita, Osaka 565-0871, Japan;
- 14 2. Immunology Frontier Research Center, Osaka University, Suita, Osaka
15 565-0871, Japan
- 16 3. Department of Pathology and Immunology, Baylor College of Medicine,
17 Houston, TX 77030.
- 18 4. Center for Drug Discovery, Baylor College of Medicine, Houston, TX
19 77030.
- 20 5. Center for Advanced Modalities and Drug Delivery System, Osaka
21 University, Osaka 565-0871, Japan
- 22 6. Center for Infectious Disease Education and Research, Osaka University,
23 Osaka 565-0871, Japan
- 24 7. The Institute of Medical Science, The University of Tokyo, Minato-ku,
25 Tokyo 108-8639, Japan.

26

27 ***Corresponding author. Email: ikawa@biken.osaka-u.ac.jp**

28 **Author Contributions:** Conceptualization: DM, MMM, and MI. Data curation: DM. Formal
29 analysis: DM. Funding acquisition: HM, MMM and MI. Methodology: DM, HM, MMM, and
30 MI. Project administration: MI. Investigation: DM, ST, HM, and MI. Visualization: DM, HM,
31 and MMM. Supervision: MI. Writing—original draft: DM and MI. Writing—review & editing:
32 All authors

33 **Competing Interest Statement:** The authors declare no conflict of interest.

34

35 **Classification:** Biological Sciences, Developmental Biology.

36 **Keywords:** Zona pellucida binding, Utero tubal junction penetration, Sterility

37

38 **This file includes:**

- 39 Main Text
- 40 Figures 1 to 7

41

42

43

44

45

46

47

48 Abstract

49 Despite the recognized importance of glycans in biological phenomena, their
50 complex roles in spermatogenesis and sperm function remain unclear. SLC35G3, a 10-
51 transmembrane protein specifically found in early round spermatids, belongs to the sugar-
52 nucleotide transporter family, indicating its involvement in glycan formation. In this
53 study, we found that *Slc35g3* knockout male mice were sterile due to impaired sperm
54 functions in uterotubal junction passage, zona pellucida binding, and oocyte fusion.
55 Mouse SLC35G3 has UDP-GlcNAc transporter activity, and its ablation caused abnormal
56 processing of the sperm plasma membrane and acrosome membrane proteins. Reported
57 human *SLC35G3* mutations (F267L and T179HfsTer27) diminished the UDP-GlcNAc
58 transporter activity of SLC35G3, implying infertility risks in males carrying these
59 mutations. Our findings unveil the vital roles of SLC35G3 in the glycan formation of
60 sperm membrane proteins critical for sperm fertilizing ability.

63 Introduction

64 Glycosylation is a post-translational modification that ensures target protein
65 synthesis, secretion, stability, characterization, and/or function (1-3). In the endoplasmic
66 reticulum (ER), the oligosaccharyltransferase complex (OSTC) co-translationally
67 transfers core glycans assembled on dolichol phosphate to asparagine residues of nascent
68 proteins. Subsequently, these proteins undergo a quality control process in which the core
69 glycan structure is processed by glucosidases, resulting in a monoglucosylated form that
70 binds to ER lectin chaperones, calnexin (CANX) and calreticulin (CALR). Once disulfide
71 bonds are correctly formed by protein disulfide isomerase (PDI) and the protein is
72 properly folded, the protein is transported to the Golgi (4, 5). Notably, there are testis-
73 specific proteins that are required for these processes and the regulation of sperm
74 fertilizing ability. Recent studies suggest that FREY tightly interacts with proteins
75 involved in N-glycosylation, and its disruption destabilizes OSTC and causes subsequent
76 ablation of the acrosomal membrane proteins essential for sperm-egg fusion (6, 7). In
77 addition to the CANX/CALR/PDI complex in somatic cells, their testis-specific paralogs,
78 CLGN/CALR3/PDILT, are required for ADAM3 sperm membrane glycoprotein
79 maturation to equip sperm fertilization competence, including the ability to pass through
80 the uterotubal junction (UTJ) (8). In the ER to Golgi secretory pathway, more than 200
81 glycosyltransferases, such as mannosyl (alpha-1,3-)-glycoprotein beta-1,2-N-
82 acetylglucosaminyltransferase (MGAT) and N-acetylgalactosaminyltransferase
83 (GALNT), add further diversity by conferring various properties, such as solubility and
84 adhesiveness to the proteins. Once glycoproteins reach the cell surface, some are secreted
85 to form the extracellular matrix, while others remain and contribute to cell adhesion and
86 interactions with substrates or other cells. Among these glycosyltransferase-like proteins,
87 DPY19L2 (a probable C-mannosyltransferase), MGAT4D, MGAT4E, MGAT4F, and
88 GALNTL5 show testis-specific expression by *in silico* analysis (9). *Dpy19l2* knockout
89 mice are infertile due to globozoospermia (10) and mutation in *Galntl5* resulted in
90 asthenozoospermia (11). Of note, GALNTL5 does not exhibit transferase activity *in vitro*
91 (12). While *Mgat4d* knockout mice are fertile (13), *Mgat4e* and *Mgat4f* orthologs do not
92 exist in humans, and their knockout mice need to be generated to reveal if they have
93 indispensable or redundant functions in mice. Collectively, these findings suggest that the
94 spermatogenic cells have a unique system for the production and quality control of

95 glycoproteins and some of them are critical for spermatogenesis, sperm functions, and
96 male fertility.

97 In the present study, we focused on the solute carrier (SLC) 35 family of
98 nucleotide sugar transporters, which are responsible for importing sugars that serve as
99 substrates for glycosyltransferases. Sugars are conjugated to nucleotides and transported
100 by specific SLC35 family antiporters into the ER and Golgi apparatus, where
101 glycosyltransferases utilize them to modify target proteins. Glycan structures are
102 synthesized from sugars including D-glucose (Glc), D-galactose (Gal), N-acetyl-D-
103 glucosamine (GlcNAc), N-acetyl-D-galactosamine (GalNAc), L-fucose (Fuc), D-
104 glucuronic acid (GlcA), D-mannose (Man), N-acetylneuraminic acid (Neu), and D-xylose
105 (Xyl). Among the SLC35 paralogs, SLC35A1 transports CMP-Sialic Acid, SLC35A2
106 transports UDP-Gal, SLC35B4 transports UDP-GlcNAc, and SLC35C1 transports GDP-
107 Fuc (14). Of the 27 SLC35 family members, most show ubiquitous expressions,
108 including in spermatogenic cells. Notably, *in silico* analysis revealed that *Slc35g3* is the
109 only SLC35 family member specifically expressed in the testis. *Slc35g3* emerged in
110 amphibians and is conserved in primates. We elucidated the biochemical properties of
111 SLC35G3 *in vitro* and generated *Slc35g3* knockout mice to study its physiological
112 functions *in vivo*. We discovered that SLC35G3 is a spermatogenic cell-specific UDP-
113 GlcNAc transporter, and *Slc35g3* ablation results in abnormal processing of sperm
114 plasma membrane and acrosome membrane glycoproteins required for sperm fertilizing
115 ability and male fertility.

116 Results

117 SLC35G3 is expressed during late spermatogenesis and localized in the Golgi 118 apparatus

119 In mice, *Slc35g3* comprises two coding exons and is located on chromosome 11,
120 whereas it is located on chromosome 17 in humans. The TreeFam (15) data confirmed
121 the evolutionary conservation of *Slc35g3* among vertebrates (**Fig. 1A**). RT-PCR analysis
122 indicates that it is prominently expressed in the testis, beginning 21 days postpartum (**Fig.**
123 **1B**), suggesting expression from the secondary spermatocyte stage to the round spermatid
124 stage in mice. The Mammalian Reproductive Genetics Database (16) revealed that
125 *Slc35g3* is the only mouse SLC35 family that shows a testis-specific transcription pattern
126 (**Fig. S1**). A previous scRNA-seq analysis suggested that transcription of *Slc35g3*
127 initiates in round spermatids (**Fig. 1C**; Mouse Cell Atlas; 17). Both AlphaFold2 (18) and
128 TOPCONS (19) analyses supported that SLC35G3 has 10 transmembrane domains (**Fig.**
129 **1D**) likely forming a homodimer (**Fig. S2**). Immunostaining colocalizes SLC35G3 with
130 Golgi marker (GM) 130 (Golgin A2), indicating SLC35G3 localization in the Golgi of
131 mouse testicular germ cells (**Fig. 1E**).

132

133 *Slc35g3*^{-/-} mice showed male infertility

134 To investigate the roles of *Slc35g3* in male reproduction, we used CRISPR/Cas9
135 to generate a homozygous knockout mouse line (*Slc35g3*^{-/-}) with an 1804-bp deletion on a
136 hybrid B6D2 background. This deletion resulted in the loss of the entire *Slc35g3* coding
137 region (**Fig. 2A, 2B**), indicating that it should be a null allele.

138 *Slc35g3*^{-/-} mice exhibit grossly normal development, appearance, and behavior,
139 consistent with its testis-restricted expression. Absence of the *Slc35g3* mRNA and
140 SLC35G3 protein in the *Slc35g3*^{-/-} testes was verified by RNA-seq (**Fig. S3**) and western
141 blot analysis (**Fig. 2C**), respectively. The specific expression of SLC35G3 in the testis,
142 but not in epididymal sperm, suggests that its function is restricted to spermatogenesis.
143 Moreover, immunofluorescence of SLC35G3 confirmed its absence in the Golgi of
144 *Slc35g3*^{-/-} mice (**Fig. S4**). Testes of *Slc35g3*^{-/-} male mice appeared normal in both
145 appearance and weight (**Fig. 2D, 2E**; +/+ vs. -/-, two-sided Student's t-test; $P = 0.42$).
146 Despite successful copulation, as evidenced by the presence of vaginal plugs, *Slc35g3*^{-/-}
147 male mice are sterile (**Fig. 2F**; +/+ vs. -/-, two-sided Wilcoxon rank-sum test, $P = 2.87 \times$
148 10^{-10}). Examination of seminiferous tubule and epididymis sections revealed no overt
149 abnormalities (**Fig. 2G** and **Fig. S5**). Furthermore, computer-assisted sperm analysis
150 revealed no significant differences in the motility of sperm from control and *Slc35g3*^{-/-}
151 males (**Fig. S6**).

152

153 ***Slc35g3*^{-/-} -derived sperm exhibit abnormal head morphology**

154 Given the subtle morphological changes observed in *Slc35g3*^{-/-}-derived sperm
155 (**Fig. 3A**), we employed elliptic Fourier descriptors (20, 21) to characterize the entire
156 sperm head shape and conducted a principal component (PC) analysis (**Fig. 3B, 3C, 3D**).
157 Wild-type-derived sperm and *Slc35g3*^{-/-}-derived sperm could be differentiated based on
158 their PC2 analysis of the tip of the sperm heads, with *Slc35g3*^{-/-}-derived sperm displaying
159 a relatively higher PC2 value (**Fig. 3C**), indicating the lack of the hook shape in *Slc35g3*^{-/-}-
160 -derived sperm. The head shape of *Slc35g3*^{-/-}-derived sperm resembled that of sperm
161 from *Fam71f2*^{-/-} (recently renamed as *Garin1a*, Golgi-associated RAB2 interactor
162 1A)(22) mice (**Fig. S7**). However, *Slc35g3*^{-/-} mice exhibited a more severe fertility
163 phenotype compared to *Fam71f2*^{-/-} mice (average litter size = 0 and 4.4 pups/litter,
164 respectively), suggesting that sperm head morphology is not the sole cause of sterility in
165 *Slc35g3*^{-/-} mice.

166

167 ***Slc35g3*^{-/-}-derived sperm exhibit impaired zona pellucida (ZP) binding and** 168 **fertilization**

169 To further analyze the cause of infertility in *Slc35g3* null male mice, we
170 performed an in vitro fertilization (IVF) assay. We first performed conventional IVF
171 using cumulus-intact oocytes with 2×10^5 sperm/mL insemination and found no oocytes
172 fertilized with spermatozoa from *Slc35g3*^{-/-} males (**Fig. 4A**). By removing cumulus cells
173 followed by insemination (**Fig. 4B**), we found a decline in the number of *Slc35g3*^{-/-}-
174 derived spermatozoa bound to the ZP (**Fig. 4C, 4D**), no oocytes fertilized as well (**Fig.**
175 **4E**, Wilcoxon rank-sum test; $P = 0.0079$). Further study, using ZP-free oocytes preloaded
176 with Hoechst33342 (**Fig. 4F**), revealed a significantly lower number of sperm fusing the
177 oocyte compared to control *Slc35g3*^{-/-} (**Fig. 4G, H**, +/- vs. -/-, Wilcoxon rank-sum test, P
178 $= 1.71 \times 10^{-21}$). Notably, oolemma fusion and fertilization were improved with a 10 times
179 higher sperm concentration from *Slc35g3*^{-/-} males but were still significantly decreased
180 compared to the lower concentrations of sperm from controls (**Fig. S8**). Lastly, IVF

181 performed using cumulus-intact oocytes with 10 times more sperm insemination (2×10^6
182 sperm/mL) resulted in a reduced fertilization rate (45.7%, 21/46), but we succeeded in
183 obtaining 10 live pups from these fertilized eggs (**Fig. S9**). Our results indicate that
184 *Slc35g3^{-/-}*-derived sperm have defects in ZP binding and oolemma fusion ability but genomic
185 integrity is intact.

186 ***Slc35g3*-deficient mice show impaired sperm migration to the oviduct.**

187 As spermatozoa lacking ZP binding frequently cannot pass through the uterotubal
188 junction (UTJ) and reach the oviduct (8), we observed sperm UTJ passage after mating.
189 This observation was facilitated by a red fluorescence signal in the sperm tails from Tg
190 mice (CAG/*su9*-DsRed2, *Acr3*-eGFP) (23; **Fig. 5A**). Two hours after copulation with
191 wild-type female mice (**Fig. 5B**), control *Slc35g3^{+/+}*-derived sperm tail signals marked by
192 red fluorescence were observed within the oviduct (**Fig. 5C**). In contrast, *Slc35g3^{-/-}*-
193 derived sperm were found in the uterus but not in the oviduct (**Fig. 5C**). Thus, male
194 infertility of *Slc35g3^{-/-}* mice was likely caused primarily by impaired sperm passage
195 through the UTJ.

196

197 ***Slc35g3* absence causes a reduced amount and abnormal processing of sperm 198 glycoproteins.**

199 To understand the molecular mechanisms behind the disrupted sperm functions
200 of *Slc35g3^{-/-}* mice, we analyzed glycoproteins related to each process. First, we examined
201 proteins involved in acrosome formation. Immunoblot analysis of *Slc35g3^{+/+}* and *Slc35g3^{-/-}*
202 testis lysates showed a reduction in the amount of ZP binding protein 1 (ZBPB1; 24),
203 whereas Golgi-associated PDZ and coiled-coil motif containing (GOPC; 25) levels
204 remained unchanged (**Fig. 6A**). Interestingly, some bands of sperm acrosome associated
205 1 (SPACA1; 26) disappeared in *Slc35g3^{-/-}* testis lysates. SPACA1 is N-glycosylated, and
206 treatment of testis and caudal sperm lysates with peptide-N-glycosidase F (PNGase F;
207 **Fig. 6B, Fig. 6C**) resulted in comparable SPACA1 band patterns between *Slc35g3^{+/+}* and
208 *Slc35g3^{-/-}* testes but not in sperm lysates. A similar result was also reported in *Fam71f1^{-/-}*
209 (Garin1b; 22) mice, which exhibit abnormal acrosome formation.

210 Next, we examined proteins involved in ZP binding. Levels of a disintegrin and
211 metalloprotease (ADAM) 1B (27) were comparable between *Slc35g3^{+/+}* and *Slc35g3^{-/-}* in
212 the testis (**Fig. 6D**) and sperm (**Fig. 6E**). Levels of CKLF-like MARVEL transmembrane
213 domain containing (CMTM) 2A and CMTM2B (28) were reduced in *Slc35g3^{-/-}* testis
214 lysates but not in sperm. The expression pattern of ADAM3 (29, 30) was comparable
215 between *Slc35g3^{+/+}* and *Slc35g3^{-/-}* testis, yet the amount of a smaller isoform was elevated
216 in *Slc35g3^{-/-}*-derived sperm lysates, indicating aberrant processing. After PNGaseF
217 treatment of proteins, the ADAM3 band pattern was comparable between *Slc35g3^{+/+}* and
218 *Slc35g3^{-/-}* (**Fig. S10**). Given the aberrant ADAM3 band pattern was also observed in testis
219 expressed gene 101 (TEX101) knockout (31) epididymal caput sperm, we examined
220 TEX101 levels through western blot analysis; however, the amount of TEX101 was
221 comparable between *Slc35g3^{+/+}* and *Slc35g3^{-/-}* testis lysates (**Fig. 6D**). Given that the
222 testicular *Ace^{-/-}* (t-ACE; 32, 33, 34) caused aberrant localization of ADAM3, we
223 examined t-ACE levels through western blot analysis and found that the amount of t-
224 ACE was comparable between *Slc35g3^{+/+}* and *Slc35g3^{-/-}* in both testis and sperm lysates

225 (Fig. 6D, 6E). In the previous studies, lymphocyte antigen 6 family member K (*Ly6k*)^{-/-}
226 (35), *Spaca4*^{-/-} (36), and LY6/PLAUR Domain Containing 4 (*Lypd4*)^{-/-} (37) sperm showed
227 impaired ZP binding; however, the amount of ADAM3 remained normal. The amount of
228 LY6K was reduced in *Slc35g3*^{-/-} testis lysates (Fig. 6D) and the amount of SPACA4 was
229 comparable between *Slc35g3*^{+/+} and *Slc35g3*^{-/-} in both testis and sperm lysates (Fig. 6D,
230 6E). However, the amount of LYPD4 in *Slc35g3*^{-/-} testis lysates decreased, and the lower
231 molecular weight band disappeared in *Slc35g3*^{-/-}-derived sperm lysates (Fig. 6E),
232 indicating the occurrence of a protein processing error or another non-N-linked
233 oligosaccharide post-translational defect.

234 Finally, we focused on the inner acrosomal membrane proteins involved in
235 oolemma fusion. IZUMO1 is an N-glycosylated acrosome membrane protein, and the
236 first to be identified as essential for sperm-oolemma fusion using knockout mice (38).
237 The levels of IZUMO1 decreased in both the testis and sperm of *Slc35g3*^{-/-} mice.
238 Although the amount of IZUMO1 in sperm was less, we did not see any other bands in
239 the western blot analysis. IZUMO1 could relocate to the equatorial segment where fusion
240 occurs after the acrosome reaction in *Slc35g3*^{-/-} derived spermatozoa (Fig. S11).
241 Equatorin (EQTN) is an O-linked glycosylated protein on the inner acrosomal membrane,
242 not essential for oolemma fusion but rather functions in oolemma binding. The EQTN
243 signal showed no difference between *Slc35g3*^{+/+} and *Slc35g3*^{-/-} testes, but it disappeared in
244 *Slc35g3*^{-/-}-derived sperm. Intriguingly, mass spectrometry analysis of sperm lysates
245 showed comparable quantitative values of EQTN between *Slc35g3*^{+/+} and *Slc35g3*^{-/-} mice
246 (Table S1). With the fact that the anti-EQTN antibody MN9 recognizes both peptide and
247 glycan structures and that the glycan structure (39), our data suggests that EQTN
248 glycosylation is aberrant in *Slc35g3*^{-/-}-derived sperm. SPACA6 is known to be lost from
249 all the sperm-oolemma fusion defective sperm (i.e., *Dcst1/2*, *Fimp*, *Izumo1*, *Sof1*,
250 *Spaca6*, and *Tmem95* knockout models) (40); however, we did not see any difference in
251 the intensity and band pattern using western blot analysis.

252

253 ***Slc35g3*^{-/-}-derived spermatozoa show impaired glycan structures**

254 To analyze the protein glycosylation status during spermatogenesis, we
255 performed lectin blot analyses using testis lysates (Fig. 7A). The band patterns of
256 concanavalin A (ConA; detecting mannose), *Aleuria aurantia* lectin (AAL; detecting
257 fucose), and *Maackia amurensis* II (MAL-II; detecting sialic acid + core1 structure) were
258 comparable between *Slc35g3*^{+/+} and *Slc35g3*^{-/-} samples. Notably, with PNA which detects
259 galactose β1-3 acetyl galactosamine (core 1 structure), the intensity of a band around 60
260 kDa increased in *Slc35g3*^{-/-} testis. As PNA binding is known to be inhibited by any
261 galactose modifications (41), the core 1 modifications might be disrupted in the target
262 protein. With *Laetiporus sulphureus* lectin N-terminal domain (LSL-N; detecting
263 LacNAc: galactose-GlcNAc), signal intensities for small proteins decreased. Intriguingly,
264 the difference became evident when we performed lectin blot analysis using mature
265 spermatozoa. Some major signals disappeared in PNA and LSL-N blot analysis (Fig.
266 7B).

267 **Mouse (m) *Slc35g3* overexpression restored glycan levels in HEK293T cells without** 268 **human (h) *SLC35B4***

269 To investigate whether SLC35G3 acts as a UDP-GlcNAc transporter, we
270 performed rescue experiments with HEK293T cells. First, we designed two gRNAs to
271 knock out *hSLC35B4* encoding a known UDP-N-acetylglucosamine (UDP-GlcNAc)
272 transporter that is highly expressed in HEK293T cells (**Fig. S12A**). The *hSLC35B4*
273 knockout cells were obtained by transfecting pX459 containing two gRNAs and
274 puromycin-resistant cassette, followed by puromycin treatment (**Fig. S12B**). After three
275 passages, the cells were transfected with a plasmid expressing *mSlc35b2* (encoding a
276 phosphoadenosine phosphosulfate transporter), *mSlc35b4*, or *mSlc35g3*-mCherry. We
277 found that the introduction of *mSlc35b2* did not rescue the amounts of proteins with
278 GlcNAc modification (**Fig. 7C**). Conversely, transfection with the *mSlc35b4*-expressing
279 plasmid rescued GlcNAc modification levels. Further, the LSL-N signals were rescued
280 by *mSlc35g3* transfection (**Fig. 7C**), suggesting that mSLC35G3 functions as a UDP-
281 GlcNAc transporter.

282

283 **T179HfsTer27 and F267L mutants failed to rescue glycan loss in *hSLC35B4*-** 284 **disrupted cells**

285 Among the frameshift mutations found in human genomes (n= 76156, gnomAD;
286 42), T179HfsTer27 frame mutation has a relatively high allele frequency ($1.88e^{-3}$), and
287 homozygous mutations are observed in 54 individuals (29 females and 25
288 males). Moreover, AlphaMissense (43), a deep learning model trained on protein
289 sequences and annotations of pathogenicity, predicted 35 pathogenic missense mutations
290 in the *hSLC35G3* gene. Among these, two mutations (F215L and F267L) were identified
291 in human genomes, and we focused on F267L, which showed potential detrimental
292 effects according to the evolutionary conservation and protein 3D structure (PolyPhen-2;
293 44). PCR and subsequent direct sequencing confirmed that the *hSLC35G3* expression
294 plasmid (wild-type, FS, or F267L) was introduced into *hSLC35B4*^{-/-} cells. With lectin blot
295 analysis using LSL-N, the signal decreased by *hSLC35B4*^{-/-} was rescued by the
296 introduction of wild-type *hSLC35G3*, while no signal recovery was observed upon the
297 introduction of FS or F267L (**Fig. 7D**). The band patterns of ConA modification
298 remained consistent across all transfected cells. These findings suggest a loss of function
299 in the T179HfsTer27 and F267L mutations.

300

301

302

303

304

304 **Discussion**

305 In this study, we identified SLC35G3 as a testis-specific UDP-GlcNAc
306 transporter to underpin proper sperm glycoprotein synthesis and functions. Although
307 *Slc35g3*^{-/-} male mice are viable, healthy, and produce motile sperm, they are completely
308 infertile, revealing a critical and unique role of SLC35G3 for producing functional
309 spermatozoa and male fertility. In vitro studies further implicated latent male infertility
310 due to *SLC35G3* mutations.

311 During spermatogenesis, *Slc35b4* is expressed in earlier stages, but it decreases
312 and is replaced by *Slc35g3* in later stages (**Fig. S1**). The reason for the stage-dependent
313 usage of two transporters is unknown, but it may be related to the formation of
314 acrosomes, which are rich in glycosylated proteins, in the later stages of spermatogenesis.

315 Although our in vitro data showed no clear differences (**Fig.7C**), SLC35B4 and
316 SLC35G3 may have different activities and/or functions. Alternatively, SLC35G3 may
317 have a lower optimal temperature because spermatogenesis progresses at a lower
318 temperature (45). Considering the transcript level of *Slc35g3* in later spermatogenesis
319 stages (highest TPM=320 at round spermatid) is higher than that of *Slc35b4* in the earlier
320 stage (highest TPM=21 at spermatogonia), spermatids may simply require more UDP-
321 GlcNAc transporter activity. Further in vitro and in vivo studies will be needed to answer
322 these questions, including transgenic mice expressing *Slc35b4* under the *Slc35g3*
323 promoter and vice versa. The answer will also help us to understand why and how
324 spermatogenic cells require a certain number of paralogous genes to be expressed
325 specifically.

326 Lectin blot analyses revealed no differences in ConA signals targeting terminal
327 mannose (**Fig. 7B**), indicating the normal formation of high-mannose-type
328 oligosaccharides for N-glycan biosynthesis in the ER of *Slc35g3^{-/-}* spermatogenic cells
329 (46). For O-glycans, there was an increase in PNA signals (core 1, Gal-GalNAc) and a
330 reduction in LSL-N signals (LacNAc: Gal-GlcNAc), while no changes were observed for
331 MAL-II (sialic acid) and AAL (fucose). These findings suggest that SLC35G3 plays
332 a more important role in glycan elongation rather than core structure, and the impaired
333 elongated glycan structure affected the properties of glycoproteins and following sperm
334 morphology and functions in *Slc35g3^{-/-}* mice.

335 While spermatogenesis looked grossly normal in *Slc35g3^{-/-}* mice (**Fig. 2D, 2E,**
336 **and 2G, fig. S6**), their spermatozoa displayed multiple phenotypic abnormalities in head
337 morphology (**Fig. 3**), UTJ migration (**Fig. 5**), and fertilization (**Fig. 4**). Regarding sperm
338 head malformation, while globozoospermia results in male infertility (e.g., *Zpbp1* (24),
339 *Gopc* (25), and *Spaca1* (26) knockout mice), most of the knockout mice with only subtle
340 head malformation can produce offspring, although at lower levels (e.g., *Zpbp2* (24),
341 *Fam71f2* (22), and *Garin2-Garin5* (47) knockout mice). We found a subtle sperm head
342 malformation in *Slc35g3^{-/-}* mice, but it should not be underestimated. For example, it has
343 been shown that mutations in multiple genes synergistically worsen head morphology,
344 even in the heterozygous state (48). Although we are still far from unraveling these
345 molecular interactions, we have revealed the importance of SLC35G3-mediated UDP-
346 GlcNAc transport for ZPBP1 stabilization and SPACA1 processing. Further research is
347 warranted on individual molecules and specific glycans to better understand their
348 relationship during sperm head morphogenesis.

349 *Slc35g3^{-/-}*-derived spermatozoa exhibited defective UTJ passage (**Fig. 5**) and ZP
350 binding (**Fig. 4D**). These defects are commonly linked and observed in many infertile
351 knockout mice, and ADAM3 is absent from most of these knockout spermatozoa (37,
352 49). However, ADAM3 is present in the *Slc35g3^{-/-}*-derived spermatozoa as in four other
353 knockout mouse lines that show the same phenotype (i.e., *Ly6k*, *Pgap1*, *Spaca4*, and
354 *Lypd4* knockout lines). These results suggest that ADAM3 may be dysfunctional in these
355 mutant sperm, or that there may be an unknown factor responsible for UTJ passage and
356 ZP binding. Because LY6K and PGAP1 only function in the testis and disappear from
357 mature spermatozoa, so we analyzed the presence of LYPD4 and SPACA4 in mature
358 spermatozoa and found that, there was abnormal processing of LYPD4 in *Slc35g3^{-/-}*-
359 derived spermatozoa (**Fig. 6E**) compared to WT sperm (50). Since ADAM3 is no longer
360 active in humans, more attention needs to be paid to LYPD4 to understand the sperm
361 fertilizing ability.

362 We next focused on the inner acrosomal membrane proteins because *Slc35g3^{-/-}*-
363 derived spermatozoa were defective in fusing with oocytes (**Fig. 6D, 6E**). While we did

364 not see any differences in SPACA6 western blot analysis, we found a decrease of
365 IZUMO1 in *Slc35g3*^{-/-}-derived spermatozoa, which is consistent with our previous study
366 showing the lack of glycosylation accompanied by a decrease in IZUMO1 levels and a
367 reduction in the number of pups (51). Intriguingly, while EQTN was detected by MS
368 analysis (**Table S1**), signals disappeared in our western blot analysis using an antibody
369 recognizing EQTN O-glycans (37; **Fig. 6E**), suggesting the presence of EQTN protein
370 without O-glycans. As *Eqtn* knockout spermatozoa decreased their oolemma binding
371 ability (37), EQTN glycans may directly contribute to oolemma binding. These results
372 suggest that SLC35G3 regulates sperm-oolemma fusion through O-linked glycosylation
373 of inner acrosomal membrane proteins.

374 Finally, we examined mutations in human *SLC35G3* for their potential risk of
375 male infertility. An in vitro study revealed that the T179HfsTer27 (17-35193772-GT-G)
376 mutation lost sugar-nucleotide transporter activity. According to gnomAD, its frequency
377 is 1.88×10^{-3} and 54 individuals have been identified as homozygous. In addition, the
378 observed/expected ratio of single nucleotide variants causing loss of function was 0.53,
379 suggesting the presence of selective pressure due to mutations. Assessment of their sperm
380 fertilizing ability would be beneficial to understanding glycosylated protein synthesis and
381 functions in human spermatozoa. Even if the mutation caused male infertility, as we
382 obtained healthy offspring by IVF with higher concentration sperm insemination,
383 intracytoplasmic sperm injection might not be necessary for their treatment.

384 In conclusion, our research suggests that SLC35G3 functions as a testis-specific
385 UDP-GlcNAc transporter during late spermatogenesis. We reaffirmed that glycosylation-
386 related genes specific to the testis play a crucial role in the synthesis, quality control, and
387 function of glycoproteins on sperm, which are essential for male fertility through their
388 interactions with eggs and the female reproductive system. Furthermore, we
389 demonstrated that human SLC35G3 also exhibits transporter activity, and proposed a loss
390 of function mutations that may cause male infertility. Further research on this gene and
391 sperm glycoprotein synthesis has the potential to contribute to understanding the causes
392 of male infertility, developing treatments, and advancing contraceptive methods.

393
394

395 **Methods**

396
397

397 **Experimental design**

398 In this study, we developed an integrated approach, combining *in silico* analysis
399 with experimental techniques, to elucidate the functions of SLC35G3. To generate
400 *Slc35g3* knockout (*Slc35g3*^{-/-}) male mice, we used the CRISPR/Cas9 system and
401 conducted *in silico* analysis for off-target/cleavage activity. Male fertility assessment
402 encompasses mating with females, alongside IVF assays. Based on the preliminary
403 literature on the SLC35 family, SLC35G3 is hypothesized to be a nucleotide sugar
404 transporter. Therefore, we performed lectin blot analysis using tissue lysate/HEK293T
405 cell lysate.

406
407

407 **Animals**

408 The manuscript adhered to the ARRIVE guidelines 2.0 for reporting. This study
409 was performed following the standards outlined in the Guide for the Care and Use of
410 Laboratory Animals. All animal experiments were approved by the Animal Care and Use
411 Committee of the Research Institute for Microbial Diseases at Osaka University, Osaka,
412 Japan (#Biken-AP-H30-01). The mice used in the study were sourced from Japan SLC,

413 Inc. (Shizuoka, JP) and were bred under specific pathogen-free conditions. They were
414 housed at 23°C, with a relative humidity of 50%, and a 12-h dark/12-h light cycle, with
415 unrestricted access to water and commercial food pellets *ad libitum*. All genetically
416 modified mice produced in this study will be accessible through either the RIKEN
417 BioResource Research Center in Ibaraki, Japan, or the Center for Animal Resources and
418 Development (CARD) at Kumamoto University, Japan.

419

420

***In silico* analysis**

421

422

423

424

425

426

427

428

429

430

RNA isolation and reverse transcription polymerase chain reaction

431

432

433

434

435

436

437

438

439

Visualization using fluorescence

440

441

442

443

444

445

446

447

448

Generation of *Slc35g3* knockout mice

449

450

451

452

453

454

455

456

457

458

459

460

461

Slc35g3 knockout mice were generated using the CRISPR/Cas9 system. Guide RNA design and potential off-target analysis were performed using the software programs CRISPRdirect (<https://crispr.dbcls.jp/>) and CRISPOR (<https://crispor.tefor.net/>). Fertilized eggs were obtained from the oviducts of super-ovulated B6D2F1 females, which were then mated with BDF1 males. Ribonucleoprotein (RNP) complexes, comprising synthesized CRISPR RNA (crRNA), trans-activating crRNA (tracrRNA), and CAS9 protein, were introduced into fertilized eggs using a NEPA21 super electroporator (Nepa Gene Co., Ltd, Chiba, JP). The treated eggs were cultured in potassium simplex optimization medium containing amino acids (KSOMaa) until the two-cell stage and were subsequently transplanted into the oviducts of 0.5-day pseudopregnant ICR females. The identity of the pups was confirmed by PCR and Sanger sequencing. Guide RNA and primer sequences are listed in **Table S2**.

462
463
464
465
466
467
468
469
470
471
472
473
474
475
476
477
478
479
480
481
482
483
484
485
486
487
488
489
490
491
492
493
494
495
496
497
498
499
500
501
502
503
504
505
506
507
508
509

***In vivo* male fertility test**

Each 8-week-old male, carrying either the *Slc35g3* wild-type or mutated gene, was individually housed with three 8-week-old B6D2F1 female mice for 2 months. Daily observations were made to identify mating plugs, and the number of resultant pups was recorded. A minimum of three males were included in each experimental group for statistical analysis.

Histological analysis of testis

Testes were dissected, fixed in Bouin's fluid (Polysciences, Warrington, PA, USA), and embedded in paraffin wax. Subsequently, 5- μ m-thick sections were obtained from the paraffin blocks using a Microm HM325 microtome (Microm, Walldorf, DE, Germany). The sections were sequentially dehydrated with xylene and ethanol, followed by a 15-minute incubation in a 1% periodic acid solution. After washing under running water for 15 min, the sections were treated with Schiff's reagent (FUJIFILM Wako, Osaka, JP) for 30 min and then stained with Mayer's hematoxylin solution for 3 min after an additional 15-min wash. Following these processes, the stained samples were observed using SLIDEVIEW VS200 (Olympus, Tokyo, JP).

Morphological analysis of sperm

Elliptical Fourier transform analysis was performed as previously described (20, 21). Briefly, photographs of the spermatozoa were captured using a microscope equipped with a complementary metal oxide semiconductor (CMOS) camera (BX53, DP74, Olympus). The sperm head shape was manually tracked from the photographs, and the elliptic Fourier analysis was performed using Momocs, a contour analysis package of the statistical analysis software R x64 4.1.2(<https://www.r-project.org/>). Top PC1-3 scores were visualized using a custom Python code.

***In vitro* fertilization**

In vitro fertilization was performed according to the previously established procedures (7). Cauda epididymal spermatozoa were dispersed in a drop of Toyoda, Yokoyama, Hoshi (TYH) medium (53) covered with paraffin oil (26117-45, Nacalai Tesque Inc., Kyoto, JP) for 2 h at 37°C under 5% CO₂ to facilitate capacitation. Eggs obtained from the oviducts of superovulated females were placed in TYH drops. Cumulus cells were removed by treating the oocytes with 330 μ g/mL of hyaluronidase (FUJIFILM Wako Pure Chemical Corp., Osaka, JP) for 5 min. To eliminate the ZP, eggs were treated with 1 mg/mL collagenase (C1639, Merck KGaA, Darmstadt, DE, Germany) for 5 min. The capacitated spermatozoa were introduced into a drop containing cumulus-intact, cumulus-free, or ZP-free eggs at a final concentration of 2×10^5 or 2×10^6 spermatozoa/mL. Pronuclei formation was observed 8 hours after insemination.

Computer-assisted sperm analysis

Sperm velocity was analyzed as previously described (54). Cauda epididymal spermatozoa were dispersed in 100 μ L drops of TYH medium. Sperm motility parameters were measured using the CEROS II sperm analysis system (software version 1.4; Hamilton Thorne Inc., Beverly, MA, USA) at 10 min and 2 h after incubation at 37°C under 5% CO₂. More than 200 spermatozoa were analyzed from each male.

Assessment of sperm passage through the utero-tubal junction

510 The assay was performed as previously described (31). Briefly, B6D2F1 female
511 mice were subjected to superovulation through intraperitoneal injection of 5 U of equine
512 chorionic gonadotropin (CG), followed by an additional 5 U of human CG (hCG) 48 h
513 later. After 12 h of hCG injection, superovulated females were placed in cages with test
514 males and vaginal plug formation was monitored at 30-min intervals. Upon confirmation
515 of plug formation, the males were separated from the females. After approximately 2 h of
516 plug formation, the oviducts, along with the connecting portion of the uterus, were
517 excised. These tissues were mounted on slides as whole specimens, covered with
518 coverslips, and examined using fluorescence microscopy (BZ-X810; Keyence
519 Corporation, Osaka, JP) to assess the presence of sperm containing the mitochondrial
520 DsRed2 marker.

521

522 **Plasmid construction**

523 The cDNAs encoding *mSlc35g3*, *mSlc35b2*, and *mSlc35b4* were amplified from
524 mouse testis (C57BL/6N), whereas the cDNA encoding *hSLC35G3* was amplified from a
525 human testis cDNA template (Quick Clone#637209, Takara Bio USA Inc., San Jose, CA,
526 USA). The T179HfsTer27 and F267L cDNA mutants were generated using the
527 *hSLC35G3* amplicon with the KOD Plus Mutagenesis Kit (SMK-101, TOYOBO Co.
528 LTD, Osaka, JP) following the manufacturer's protocol. The *mSlc35g3* cDNA was
529 inserted into the mCherry-tagged (C-terminus) pCAG vector, whereas the *mSlc35b2*,
530 *mSlc35b4*, *hSLC35G3*, T179HfsTer27, and F267L cDNAs were cloned into the pCAG
531 vector containing the CAG promoter and rabbit globin poly (A) signal, as previously
532 described (55). The primers used to construct these plasmids are listed in Table S2.

533

534 **Cell culture and transfection**

535 HEK293T cells (56) were cultured in DMEM (11995–065, Thermo Fisher
536 Scientific) supplemented with 10% fetal bovine serum (S1560, BioWest, Nuaille, FR)
537 and 1% penicillin-streptomycin-glutamine (10378–016, Thermo Fisher Scientific) at
538 37°C under 5% CO₂. Subsequently, these cells were transiently transfected with the
539 plasmid DNA and cultured.

540

541 **Western blot analysis/lectin blot analysis**

542 Immunoblotting procedures closely followed those described previously
543 (57). Testis, spermatozoa from the cauda epididymis, and collected cells were immersed
544 in lysis buffer (1% Triton X-100, 50 mM Tris-HCl pH 7.5, 150 mM NaCl) supplemented
545 with a protease inhibitor cocktail (Cat. No. 25955, Nacalai Tesque Inc.) and left to
546 incubate overnight at 4°C. Subsequently, the lysate was centrifuged at 10 000 × g for 15
547 min at 4°C. The resulting supernatants were used for either lectin precipitation or SDS-
548 PAGE for immunoblot or lectin blot analysis. PNGase F (P0704S, New England Biolabs
549 Inc., Ipswich, MA, USA) was applied to the testis and sperm lysates to enzymatically
550 treat the glycosidases, following the manufacturer's guidelines.

551

552 For lectin blot analysis, a blocking solution (10 mM Tris-HCl, 0.15 M NaCl,
553 0.05% Tween 20) was employed instead of skim milk for immunoblot analysis. The
554 primary antibody was replaced with biotin-conjugated lectin, and the secondary antibody
555 was substituted with HRP-conjugated streptavidin. The pertinent antibodies and lectins
556 are listed in Table S3.

557

558 For lectin precipitation, supernatants from the testis were incubated with lectin-
biotin overnight at 4°C, followed by incubation with streptavidin-conjugated Dynabeads
(Cat. No. 65001, Thermo Fisher Scientific) for 1 h at room temperature. After three

559 washes with a mild buffer (42 mM Tris-HCl pH 7.5, 150 mM NaCl, 0.1% Triton X-100,
560 and 10% glycerol), the complexes were eluted using a sample buffer containing 2-
561 mercaptoethanol.

562

563 **Mass spectrometry**

564 The samples were subjected to mass spectrometry analysis as previously
565 described (57). “The proteins were reduced with 10 mM dithiothreitol (DTT), followed
566 by alkylation with 55 mM iodoacetamide, and digested in-gel by treatment with trypsin
567 and purified with C18 tip (GL-Science, Tokyo, Japan). The resultant peptides were
568 subjected to nanocapillary reversedphase LC-MS/MS analysis using a C18 column (25
569 cm × 75 μm, 1.6 μm; IonOpticks, Victoria, Australia) on a nanoLC system (Bruker
570 Daltoniks, Bremen, Germany) connected to a timsTOF Pro mass spectrometer (Bruker
571 Daltoniks) and a modified nano-electrospray ion source (CaptiveSpray; Bruker
572 Daltoniks). The mobile phase consisted of water containing 0.1% formic acid (solvent A)
573 and acetonitrile containing 0.1% formic acid (solvent B). Linear gradient elution was
574 carried out from 2% to 35% solvent B for 18 min at a flow rate of 400 nL/min. The ion
575 spray voltage was set at 1.6 kV in the positive ion mode. Ions were collected in the
576 trapped ion mobility spectrometry (TIMS) device over 100 ms and MS and MS/MS data
577 were acquired over an m/z range of 100-1,700. During the collection of MS/MS data, the
578 TIMS cycle was adjusted to 1.1 s and included 1 MS plus 10 parallel accumulation serial
579 fragmentation (PASEF)-MS/MS scans, each containing on average 12 MS/MS spectra
580 (>100 Hz), and nitrogen gas was used as collision gas.” Protein identification was carried
581 out using Mascot (version: 2.7.0; Matrix Science, London, UK) regarding
582 Scaffold_4.10.0 (Proteome Software Inc., Portland, OR, USA). Human keratin peptides
583 were excluded from the analysis.

584

585 **Statistical analysis**

586 Normality was assessed using the Shapiro–Wilk normality test, and variance was
587 examined using the F-test. Non-parametric tests were performed using the Wilcoxon
588 rank-sum test, whereas parametric tests were performed using the two-tailed Student's t-
589 test or Welch's t-test. All statistical analyses were performed using R x64 4.1.2
590 (<https://www.r-project.org/>). Significance levels were established at *P<0.05, **P<0.01,
591 and ***P<0.001. Data are presented as mean ± standard deviation (s.d.). Quantified data
592 were visualized as dot plots using PlotsofData (58
593 <https://huygens.science.uva.nl/PlotsOfData/>) or custom Python code in Google Colab
594 (<https://colab.research.google.com/>).

595

596

597

598

599

600 **References**

601

602 1. Matzuk, M.M. and Boime, I. The role of the asparagine-linked
603 oligosaccharides of the a subunit in the secretion and assembly of human
604 chorionic gonadotropin. *J. Cell Biol.* 106, 1049-1059 (1988).

605 2. Matzuk, M.M., Keene, J.L., and Boime, I. Site specificity of the
606 chorionic gonadotropin N-linked oligosaccharides in signal transduction. *J. Biol.*
607 *Chem.* 264, 2409-2414 (1989).

- 608 3. Schjoldager, K. T., Narimatsu, Y., Joshi, H. J., & Clausen, H. (2020).
609 Global view of human protein glycosylation pathways and functions. *Nature*
610 *reviews Molecular cell biology*, 21(12), 729-749.
- 611 4. Tannous, A., Pisoni, G. B., Hebert, D. N., & Molinari, M. (2015, May).
612 N-linked sugar-regulated protein folding and quality control in the ER. In
613 *Seminars in cell & developmental biology* (Vol. 41, pp. 79-89). Academic Press.
- 614 5. Ikawa, M., Wada, I., Kominami, K., Watanabe, D., Toshimori, K.,
615 Nishimune, Y., & Okabe, M. (1997). The putative chaperone calmeglin is
616 required for sperm fertility. *Nature*, 387(6633), 607-611.
- 617 6. Contreras, W., Wiesehöfer, C., Schreier, D., Leinung, N., Peche, P.,
618 Wennemuth, G., ... & Mentrup, T. (2022). C11orf94/Frey is a key regulator for
619 male fertility by controlling Izumo1 complex assembly. *Science Advances*, 8(31),
620 eabo6049.
- 621 7. Lu, Y., Shimada, K., Tang, S., Zhang, J., Ogawa, Y., Noda, T., ... &
622 Ikawa, M. (2023). 1700029I15Rik orchestrates the biosynthesis of acrosomal
623 membrane proteins required for sperm-egg interaction. *Proceedings of the*
624 *National Academy of Sciences*, 120(8), e2207263120.
- 625 8. Tokuhiko, K., Ikawa, M., Benham, A. M., & Okabe, M. (2012). Protein
626 disulfide isomerase homolog PDILT is required for quality control of sperm
627 membrane protein ADAM3 and male fertility. *Proceedings of the National*
628 *Academy of Sciences*, 109(10), 3850-3855.
- 629 9. Oura, S., Mori, H., & Ikawa, M. (2022). Genome editing in mice and its
630 application to the study of spermatogenesis. *Gene and Genome Editing*, 3,
631 100014.
- 632
- 633 10. Pierre, V., Martinez, G., Coutton, C., Delaroche, J., Yassine, S., Novella,
634 C., ... & Arnoult, C. (2012). Absence of Dpy19L2, a new inner nuclear membrane
635 protein, causes globozoospermia in mice by preventing the anchoring of the
636 acrosome to the nucleus. *Development*, 139(16), 2955-2965.
- 637 11. Takasaki, N., Tachibana, K., Ogasawara, S., Matsuzaki, H., Hagiuda, J.,
638 Ishikawa, H., ... & Narimatsu, H. (2014). A heterozygous mutation of GALNTL5
639 affects male infertility with impairment of sperm motility. *Proceedings of the*
640 *National Academy of Sciences*, 111(3), 1120-1125.
- 641 12. Lu, Y., Oura, S., Matsumura, T., Oji, A., Sakurai, N., Fujihara, Y., ... &
642 Ikawa, M. (2019). CRISPR/Cas9-mediated genome editing reveals 30 testis-
643 enriched genes dispensable for male fertility in mice. *Biology of Reproduction*,
644 101(2), 501-511.
- 645 13. Raman, J., Guan, Y., Perrine, C. L., Gerken, T. A., & Tabak, L. A.
646 (2012). UDP-N-acetyl- α -D-galactosamine: polypeptide N-
647 acetylgalactosaminyltransferases: completion of the family tree. *Glycobiology*,
648 22(6), 768-777.
- 649 14. Ahuja, S., & Whorton, M. R. (2019). Structural basis for mammalian
650 nucleotide sugar transport. *Elife*, 8, e45221.
- 651 15. J. Ruan, H. Li, Z. Chen, A. Coghlan, L. J. M. Coin, Y. Guo, J. K.
652 Hériché, Y. Hu, K. Kristiansen, R. Li, T. Liu, A. Moses, J. Qin, S. Vang, A. J.
653 Vilella, A. Ureta-Vidal, L. Bolund, J. Wang, R. Durbin, TreeFam: 2008 update.
654 *Nucleic Acids Res.* 36(suppl_1), D735–D740 (2007).
- 655 16. M. J. Robertson, K. Kent, N. Tharp, K. Nozawa, L. Dean, M. Mathew, S.
656 L. Grimm, Z. Yu, C. Légaré, Y. Fujihara, M. Ikawa, R. Sullivan, C. Coarfa, M.

- 657 M. Matzuk, T. X. Garcia, Large-scale discovery of male reproductive tract-
658 specific genes through analysis of RNA-seq datasets. *BMC Biol.* **18**(1), 103
659 (2020). doi: 10.1186/s12915-020-00826-z PMID: 32814578
- 660 17. R. Wang, P. Zhang, J. Wang, Ma L, W. E, S. Suo, M. Jiang, J. Li, H.
661 Chen, H. Sun, L. Fei, Z. Zhou, Y. Zhou, Y. Chen, W. Zhang, X. Wang, Y. Mei,
662 Z. Sun, C. Yu, J. Shao, Y. Fu, Y. Xiao, F. Ye, X. Fang, H. Wu, Q. Guo, X. Fang,
663 X. Li, X. Gao, D. Wang, P. F. Xu, R. Zeng, G. Xu, L. Zhu, L. Wang, J. Qu, D.
664 Zhang, H. Ouyang, H. Huang, M. Chen, S. C. Ng, G. H. Liu, G. C. Yuan, G.
665 Guo, X. Han, Construction of a cross-species cell landscape at single-cell level.
666 *Nucleic Acids Res.* **51**(1), 501–516 (2022). <https://doi.org/10.1093/nar/gkac633>
667 18. J. Jumper, R. Evans, A. Pritzel, T. Green, M. Figurnov, O. Ronneberger,
668 K. Tunyasuvunakool, R. Bates, A. Židek, A. Potapenko, A. Bridgland, C. Meyer,
669 S. A. A. Kohl, A. J. Ballard, A. Cowie, B. Romera-Paredes, S. Nikolov, R. Jain,
670 J. Adler, T. Back, S. Petersen, D. Reiman, E. Clancy, M. Zielinski, M.
671 Steinegger, M. Pacholska, T. Berghammer, S. Bodenstein, D. Silver, Vinyals. O,
672 A. W. Senior, K. Kavukcuoglu, P. Kohli, D. Hassabis, Highly accurate protein
673 structure prediction with AlphaFold. *Nature* **596**, 583–589 (2021).
674 <https://doi.org/10.1038/s41586-021-03819-2>
- 675 19. K. D. Tsirigos, C. Peters, N. Shu, L. Käll, A. Elofsson, The TOPCONS
676 web server for consensus prediction of membrane protein topology and signal
677 peptides. *Nucleic Acids Res.* **43**(W1), W401–W407 (2015).
- 678 20. F. P. Kuhl, C. R. Giardina, Elliptic Fourier features of a closed contour.
679 *Comput. Graph. Image Process.* **18**(3), 236–258 (1982).
- 680 21. D. Mashiko, M. Ikawa, K. Fujimoto, Mouse spermatozoa with higher
681 fertilization rates have thinner nuclei. *PeerJ* **5**, e3913 (2017).
682 <https://doi.org/10.7717/peerj.3913>
- 683 22. A. Morohoshi, H. Miyata, Y. Oyama, S. Oura, T. Noda, M. Ikawa,
684 FAM71F1 binds to RAB2A and RAB2B and is essential for acrosome formation
685 and male fertility in mice. *Development* **148**(21), dev199644 (2021).
- 686 23. H. Hasuwa, Y. Muro, M. Ikawa, N. Kato, Y. Tsujimoto, M. Okabe,
687 Transgenic mouse sperm that have green acrosome and red mitochondria allow
688 visualization of sperm and their acrosome reaction in vivo. *Exp. Anim.* **59**(1),
689 105–107 (2010).
- 690 24. Y. N. Lin, A. Roy, W. Yan, K. H. Burns, M. M. Matzuk, Loss of zona
691 pellucida binding proteins in the acrosomal matrix disrupts acrosome biogenesis
692 and sperm morphogenesis. *Mol. Cell Biol.* **27**(19), 6794–6805 (2007).
- 693 25. R. Yao, C. Ito, Y. Natsume, Y. Sugitani, H. Yamanaka, S. Kuretake, K.
694 Yanagida, A. Sato, K. Toshimori, T. Noda, Lack of acrosome formation in mice
695 lacking a Golgi protein, GOPC. *Proc. Natl. Acad. Sci. U. S. A.* **99**, 11211–11216
696 (2002).
- 697 26. Y. Fujihara, Y. Satouh, N. Inoue, A. Isotani, M. Ikawa, M. Okabe,
698 SPACA1-deficient male mice are infertile with abnormally shaped sperm heads
699 reminiscent of globozoospermia. *Development* **139**(19), 3583–3589 (2012).
- 700 27. E. Kim, M. Yamashita, T. Nakanishi, K. E. Park, M. Kimura, S. I.
701 Kashiwabara, T. Baba, Mouse sperm lacking ADAM1b/ADAM2 fertilin can fuse
702 with the egg plasma membrane and effect fertilization. *J. Biol. Chem.* **281**(9),
703 5634–5639 (2006).
- 704 28. Y. Fujihara, A. Oji, K. Kojima-Kita, T. Larasati, M. Ikawa, Co-
705 expression of sperm membrane proteins CMTM2A and CMTM2B is essential for

- 706 ADAM3 localization and male fertility in mice. *J. Cell Sci.* **131**(19), jcs221481
707 (2018).
- 708 29. R. Shamsadin, I. M. Adham, K. Nayernia, U. A. Heinlein, H.
709 Oberwinkler, W. Engel, Male mice deficient for germ-cell cyritestin are infertile.
710 *Biol. Reprod.* **61**(6), 1445–1451 (1999).
- 711 30. R. Yamaguchi, Y. Muro, A. Isotani, K. Tokuhira, K. Takumi, I. Adham,
712 M. Ikawa, M. Okabe, Disruption of ADAM3 impairs the migration of sperm into
713 oviduct in mouse. *Biol. Reprod.* **81**(1), 142–146 (2009).
- 714 31. Y. Fujihara, K. Tokuhira, Y. Muro, G. Kondoh, Y. Araki, M. Ikawa, M.
715 Okabe, Expression of TEX101, regulated by ACE, is essential for the production
716 of fertile mouse spermatozoa. *Proc. Natl. Acad. Sci.* **110**(20), 8111–8116 (2013).
- 717 32. J. H. Kregge, S. W. John, L. L. Langenbach, J. B. Hodgins, J. R. Hagaman,
718 E. S. Bachman, J. C. Jennette, D. A. O'Brien, O. Smithies, Male-female
719 differences in fertility and blood pressure in ACE-deficient mice. *Nature*
720 **375**, 146–148 (1995). doi: 10.1038/375146a0.
- 721 33. J. R. Hagaman, J. S. Moyer, E. S. Bachman, M. Sibony, P. L. Magyar, J.
722 E. Welch, O. Smithies, J. H. Kregge, D. A. O'Brien, Angiotensin-converting
723 enzyme and male fertility. *Proc. Natl. Acad. Sci. U. S. A.* **95**, 2552–2557 (1998).
724 doi: 10.1073/pnas.95.5.2552.
- 725 34. R. Yamaguchi, K. Yamagata, M. Ikawa, S. B. Moss, M. Okabe, Aberrant
726 distribution of ADAM3 in sperm from both angiotensin-converting enzyme
727 (Ace)—and calmeglin (Clgn)-deficient mice. *Biol. Reprod.* **75**, 760–766 (2006).
728 doi: 10.1095/biolreprod.106.052977
- 729 35. Y. Fujihara, M. Okabe, M. Ikawa, GPI-anchored protein complex,
730 LY6K/TEX101, is required for sperm migration into the oviduct and male
731 fertility in mice. *Biol. Reprod.* **90**(3), 60–61 (2014).
- 732 36. Y. Fujihara, S. Herberg, A. Blaha, K. Panser, K. Kobayashi, T. Larasati,
733 M. Novatchkova, H. C. Theussl, O. Olszanska, M. Ikawa, A. Pauli, The
734 conserved fertility factor SPACA4/Bouncer has divergent modes of action in
735 vertebrate fertilization. *Proc. Natl. Acad. Sci. U. S. A.* **118**(39), e2108777118
736 (2021).
- 737 37. Y. Fujihara, T. Noda, K. Kobayashi, A. Oji, S. Kobayashi, T.
738 Matsumura, T. Larasati, S. Oura, K. Kojima-Kita, Z. Yu, M. M. Matzuk, M.
739 Ikawa, Identification of multiple male reproductive tract-specific proteins that
740 regulate sperm migration through the oviduct in mice. *Proc. Natl. Acad. Sci. U. S.*
741 *A.* **116**(37), 18498–18506 (2019).
- 742 38. N. Inoue, M. Ikawa, A. Isotani, M. Okabe, The immunoglobulin
743 superfamily protein Izumo is required for sperm to fuse with eggs. *Nature*
744 **434**(7030), 234–238 (2005).
- 745 39. K. Toshimori, S. Araki, I. Tanii, C. Ōura, Masking the cryptodeterminant
746 on the 54-kilodalton mouse sperm surface antigen. *Biol. Reprod.* **47**(6), 1161–
747 1167 (1992).
- 748 40. T. Noda, Y. Lu, Y. Fujihara, S. Oura, T. Koyano, S. Kobayashi, M. M.
749 Matzuk, M. Ikawa, Sperm proteins SOF1, TMEM95, and SPACA6 are required
750 for sperm– oocyte fusion in mice. *Proc. Natl. Acad. Sci. U. S. A.* **117**(21), 11493–
751 11502 (2020).
- 752 41. D. Bojar, L. Meche, G. Meng, W. Eng, D. F. Smith, R. D. Cummings, L.
753 K. Mahal, A useful guide to lectin binding: machine-learning directed annotation
754 of 57 unique lectin specificities. *ACS Chem. Biol.* **17**(11), 2993–3012 (2022).

- 755 42. S. Chen, L. C. Francioli, J. K. Goodrich, R. L. Collins, M. Kanai, Q.
756 Wang, J. Alföldi, N. A. Watts, C. Vittal, L. D. Gauthier, T. Poterba, M. W.
757 Wilson, Y. Tarasova, W. Phu, M. T. Yohannes, Z. Koenig, Y. Farjoun, E. Banks,
758 S. Donnelly, S. Gabriel, N. Gupta, S. Ferriera, C. Tolonen, S. Novod, L.
759 Bergelson, D. Roazen, V. Ruano-Rubio, M. Covarrubias, C. Llanwarne, N.
760 Petrillo, G. Wade, T. Jeandet, R. Munshi, K. Tibbetts, A. O'Donnell-Luria, M.
761 Solomonson, C. Seed, A. R. Martin, M. E. Talkowski, H. L. Rehm, M. J. Daly,
762 G. Tiao, B. M. Neale, D. G. MacArthur, K. J. Karczewski, gnomAD Project
763 Consortium, A genome-wide mutational constraint map quantified from variation
764 in 76,156 human genomes. *bioRxiv* **2022-03**, PPR556342 (2022).
765 <https://doi.org/10.1101/2022.03.20.485034>
766 43. J. Cheng, G. Novati, J. Pan, C. Bycroft, A. Žemgulytė, T. Applebaum, A.
767 Pritzel, L. H. Wong, M. Zielinski, T. Sargeant, R. G. Schneider, A. W. Senior, J.
768 Jumper, D. Hassabis, P. Kohli, Ž. Avsec, Accurate proteome-wide missense
769 variant effect prediction with AlphaMissense. *Science* **381**(6664), eadg7492
770 (2023).
771 44. I. A. Adzhubei, S. Schmidt, L. Peshkin, V. E. Ramensky, A.
772 Gerasimova, P. Bork, A. S. Kondrashov, S. R. Sunyaev. *Nat Methods* **7**(4), 248–
773 249 (2010).
774 45. JM. Bedford . Effects of elevated temperature on the epididymis and
775 testis: experimental studies. *Adv Exp Med Biol.* 1991;286:19-32. doi:
776 10.1007/978-1-4684-5913-5_3. PMID: 2042501.
777 46. M. Aebi, N-linked protein glycosylation in the ER. *Biochim. Biophys.*
778 *Acta* **1833**(11), 2430–2437 (2013).
779 47. Wang, H., Iida-Norita, R., Mashiko, D., Pham, A. H., Miyata, H., &
780 Ikawa, M. (2024). Golgi associated RAB2 interactor protein family contributes to
781 murine male fertility to various extents by assuring correct morphogenesis of
782 sperm heads. *PLoS Genetics*, *20*(6), e1011337.
783 48. Martinez, G., Coutton, C., Loeuillet, C., Cazin, C., Muroňová, J.,
784 Boguenet, M., ... & Arnoult, C. (2022). Oligogenic heterozygous inheritance of
785 sperm abnormalities in mouse. *Elife*, *11*, e75373.
786 49. Fujihara, Y., Miyata, H., & Ikawa, M. (2018). Factors controlling sperm
787 migration through the oviduct revealed by gene-modified mouse models.
788 *Experimental Animals*, *67*(2), 91-104.
789 50. D. Wang, L. Cheng, W. Xia, X. Liu, Y. Guo, X. Yang, X. Guo, E. Y. Xu,
790 LYPD4, mouse homolog of a human acrosome protein, is essential for sperm
791 fertilizing ability and male fertility. *Biol. Reprod.* **102**(5), 1033–1044 (2020).
792 51. N. Inoue, M. Ikawa, M. Okabe, Putative sperm fusion protein IZUMO
793 and the role of N-glycosylation. *Biochem. Biophys. Res. Commun.* **377**, 910–914
794 (2008)
795 52. Kotaja, N., Kimmins, S., Brancorsini, S., Hentsch, D., Vonesch, J. L.,
796 Davidson, I., ... & Sassone-Corsi, P. (2004). Preparation, isolation and
797 characterization of stage-specific spermatogenic cells for cellular and molecular
798 analysis. *Nature methods*, *1*(3), 249-254.
799 53. Y. Toyoda, M. Yokoyama, T. Hosi, Studies on the fertilization of mouse
800 eggs in vitro. *Jpn. J. Anim. Reprod.* **16**, 152–157 (1971). 10.1262/jrd1955.16.152
801 54. H. Miyata, Y. Satouh, D. Mashiko, M. Muto, K. Nozawa, K. Shiba, Y.
802 Fujihara, A. Isotani, K. Inaba, M. Ikawa, Sperm calcineurin inhibition prevents

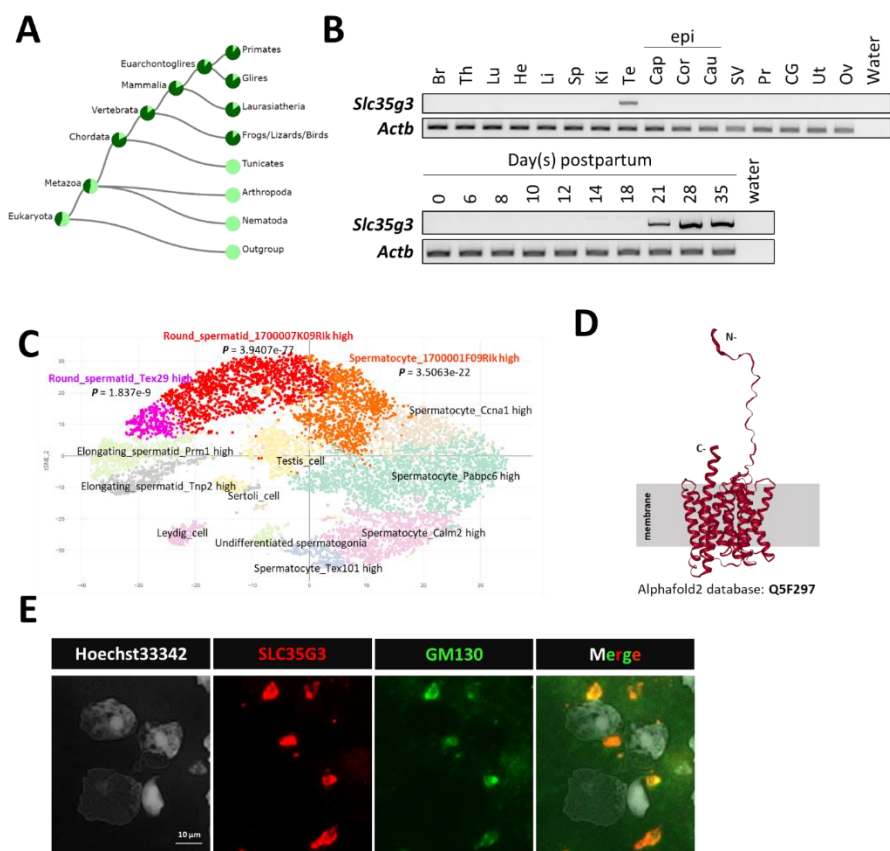
803 mouse fertility with implications for male contraceptive. *Science*, **350**(6259),
804 442–445 (2015).
805 55. H. Niwa, K. Yamamura, J. Miyazaki, Efficient selection for high-
806 expression transfectants with a novel eukaryotic vector. *Gene* **108**, 193–199
807 (1991). 10.1016/0378-1119(91)90434-D
808 56. G. Tiscornia, O. Singer, I. M. Verma, Production and purification of
809 lentiviral vectors. *Nat. Protoc.* **1**, 241–245 (2006). 10.1038/nprot.2006.37
810 57. K. Shimada, S. Park, H. Miyata, Z. Yu, A. Morohoshi, S. Oura, M. M.
811 Matzuk, M. Ikawa, ARMC12 regulates spatiotemporal mitochondrial dynamics
812 during spermiogenesis and is required for male fertility. *Proc. Natl. Acad. Sci. U.*
813 *S. A.* **118**, e2018355118 (2021). 10.1073/pnas.2018355118
814 58. M. Postma, J. Goedhart, PlotsOfData—A web app for visualizing data
815 together with their summaries. *PLoS Biol.* **17**(3), e3000202 (2019).
816
817

818 Acknowledgments

819 We express our sincere gratitude to Ms. Saki Nishioka and the NPO for Biotechnology
820 Research and Development for their valuable technical support and to the members of
821 both the Department of Experimental Genome Research and Animal Resource Center for
822 Infectious Diseases at the Research Institute for Microbial Diseases (RIMD) of Osaka
823 University, Japan for their assistance and engaging discussions during the experiments.
824 We acknowledge the RIMD NGS core facility for its valuable support in sequencing and
825 data analysis. We also thank A. Ninomiya and F. Sugihara for MS analysis (RIMD Core
826 Instrumentation Facility).

827 **Funding:** This work was financially supported by the Ministry of Education, Culture, Sports,
828 Science and Technology/Japan Society for the Promotion of Science (JP21K19569 and
829 JP22H03214 to H.M.; JP21H05033, JP22H04922 and JP23K20043 to M.I.); the Japan
830 Science and Technology Agency (JPMJFR211F to H.M.; JPMJCR21N1 to M.I.); the
831 Japan Agency for Medical Research and Development (JP23jf0126001, JP23fa627002,
832 and JP23fa627006 to M.I.); the Takeda Science Foundation (grants to H.M. and M.I.);
833 the *Eunice Kennedy Shriver* National Institute of Child Health and Human Development
834 (R01HD088412 to M.M. and M.I.); and the Bill & Melinda Gates Foundation (INV-
835 001902 to M.M. and M.I.). OU master plan (JPMXP1323015484 to M.I.)

836 **Data and material availability:** All data needed to evaluate the conclusions in the paper are
837 present in the paper and/or the Supplementary Materials. The gene-manipulated mouse
838 lines used in this study were deposited at the RIKEN BioResource Research Center
839 (RIKEN BRC, Tsukuba, Japan) and the Center for Animal Resources and Development
840 (CARD) Kumamoto University (Kumamoto, Japan). These cell lines are available
841 through these centers subject to scientific review and completion of a material transfer
842 agreement. Requests for access to genetically manipulated mice should be submitted to
843 these centers.
844
845



846

847

848

849

850

851

852

853

854

855

856

857

858

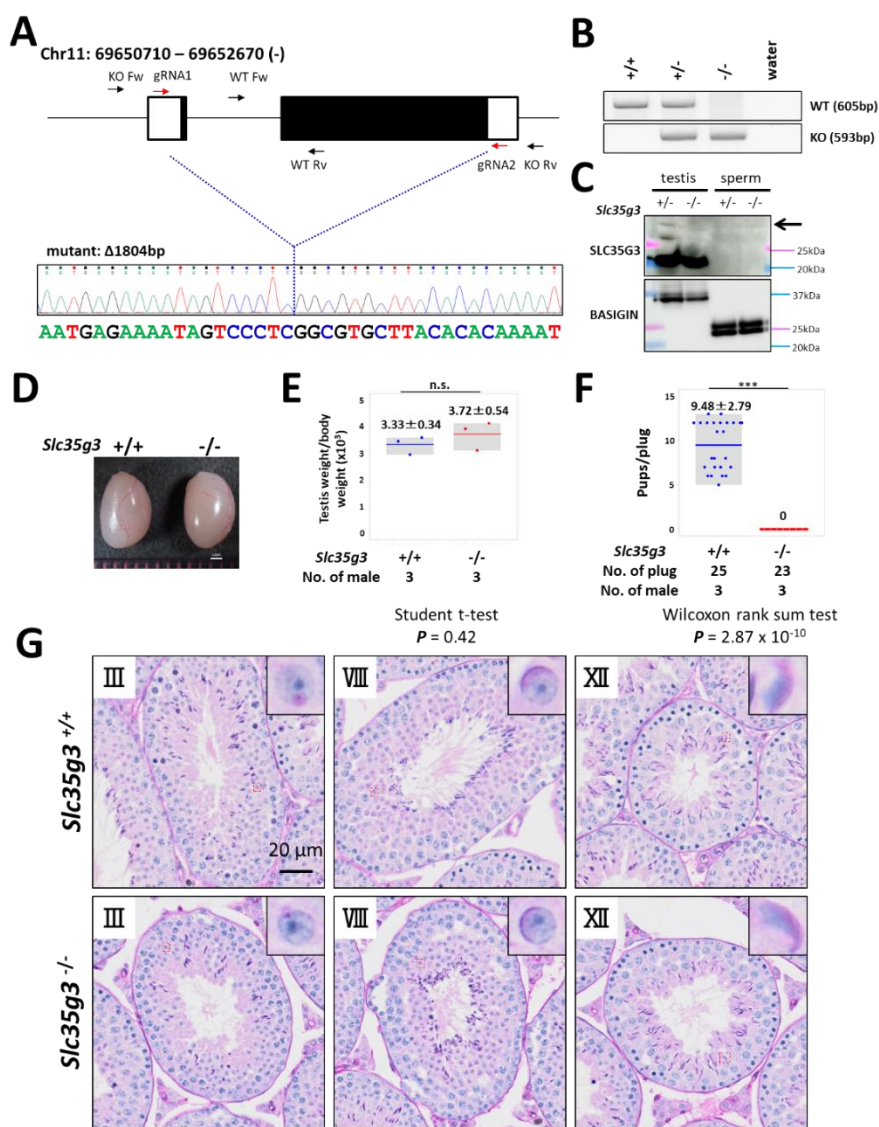
859

860

861

Fig. 1. SLC35G3 is a multi-pass transmembrane protein with unique testes-specific expression in the Golgi apparatus during early spermiogenesis.

(A) Phylogenetic tree of *Slc35g3* from the TreeFam database, with dark green areas indicating the presence and light green areas indicating the absence of *Slc35g3*. (B) RT-PCR results across multiple tissues (upper panel) and from testes at various days postpartum (lower panel); Br: brain, Th: thymus, Lu: lung, He: heart, Li: liver, Sp: spleen, Ki: kidney, Te: testis; Epi: epididymis, Cap: caput epididymis, Cor: corpus epididymis, Cau: cauda epididymis; SV: seminal vesicle, Pr: prostate, CG: coagulating gland, Ut: uterus, Ov: ovary. β -actin (*Actb*) was used as the loading control. (C) scRNA-seq prediction of cells strongly expressing *Slc35g3* mRNA (Mouse cell atlas). Dots with low transparency represent cells with predicted expression. (D) SLC35G3 structure predicted using Alpha Fold. (E) From left to right: Hoechst33342 staining image, SLC35G3 immunostaining image, GM130 immunostaining image, and merged image of wild-type testicular germ cells. Scale bar: 10 μ m



862

863

Fig. 2. *Slc35g3*^{-/-} induces male sterility.

864

(A) Depiction of *Slc35g3* gene location and structure, gRNA/primer design, and the

865

sequencing result of the mutant (deleted) allele. (B) PCR genotyping results for

866

Slc35g3^{+/+}, *Slc35g3*^{+/-}, *Slc35g3*^{-/-}, and water are presented. (C) Western blot analysis

867

results obtained with *Slc35g3*^{+/+} and *Slc35g3*^{-/-} testis lysates and *Slc35g3*^{+/+} and *Slc35g3*^{-/-}

868

derived cauda epididymal sperm lysates are shown. (D, E) Similar testis sizes (D) and

869

weights (E) from *Slc35g3*^{+/+} and *Slc35g3*^{-/-} mice (two-sided Student's t-test; $P = 0.42$).

870

(F) Comparison of the number of pups per vaginal plug between *Slc35g3*^{+/+} and *Slc35g3*^{-/-}

871

mice (Wilcoxon rank-sum test; $P = 2.87 \times 10^{-10}$). (G) Histological analysis of testis

872

sections from *Slc35g3*^{+/+} mice (upper panels) and those from *Slc35g3*^{-/-} mice (lower

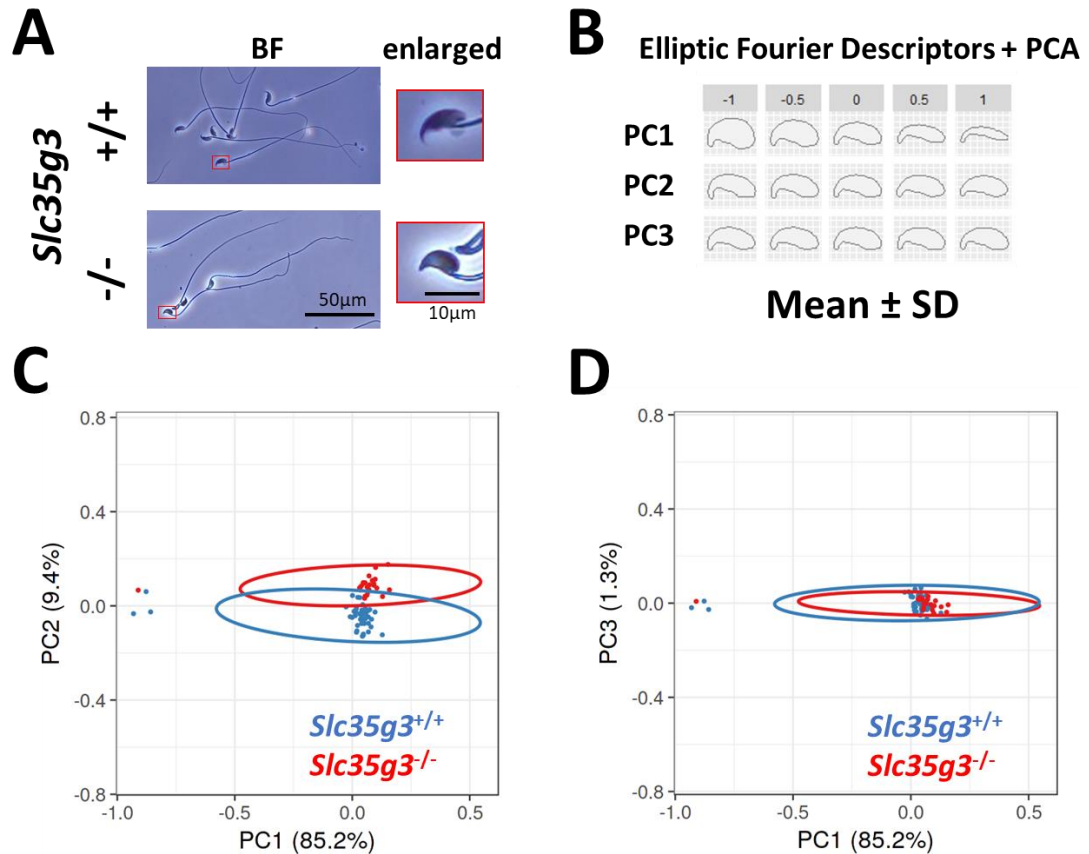
873

panels); images depict stages III (Golgi phase), VIII (acrosome phase), and XII

874

(maturation phase).

875

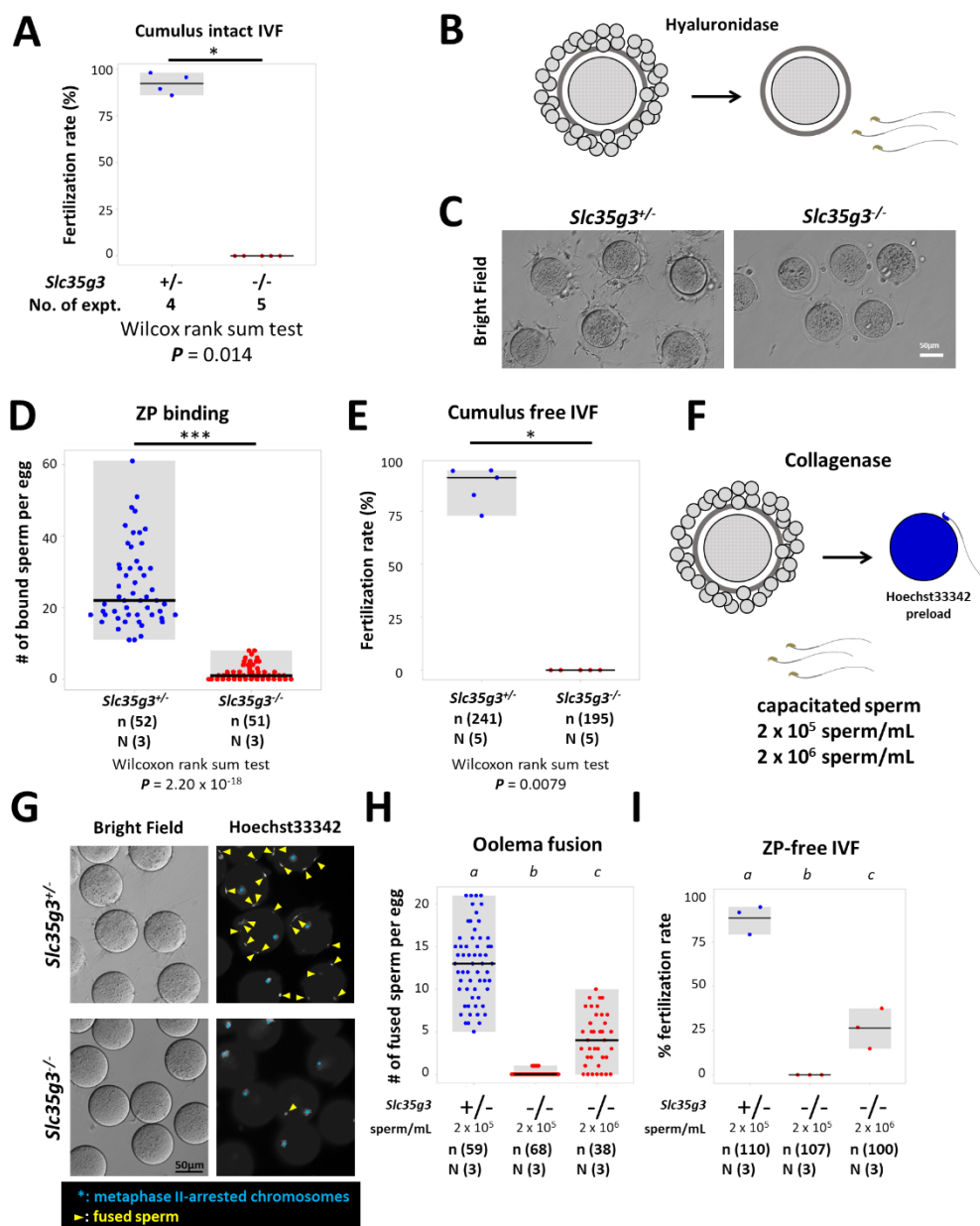


876
877

878
879
880
881
882
883
884
885
886
887

Fig. 3. *Slc35g3* is essential for sperm head formation.

(A) Bright-field (BF) views of *Slc35g3*^{+/+}-derived sperm (upper panels) versus *Slc35g3*^{-/-}-derived sperm (lower panels); red frames are images enlarged four times. Scale bar: 50 μ m for BF images, 10 μ m for enlarged ones. (B) Morphological characteristics are indicated by mean \pm SD of each principal component (PC) following elliptic Fourier analysis; the upper value represents SD, with zero indicating average morphology. (C, D) Plots of PC1-PC2 (C) and PC1-PC3 (D) coordinates of the elliptic Fourier analysis of sperm from *Slc35g3*^{+/+} mice (blue encircled) versus *Slc35g3*^{-/-} mice (red encircled); circles represent 95% confidence ellipses. Scale bar = 10 μ m.



888

889

890

891

892

893

894

895

896

897

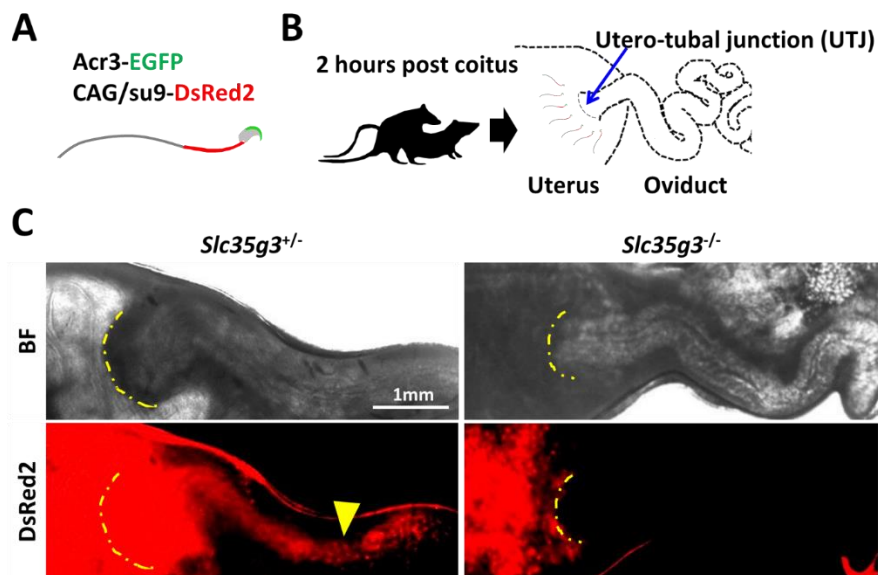
898

Fig. 4. *Slc35g3*^{-/-}-derived spermatozoa are defective in ZP binding and oolemma fusion.

(A) The IVF fertilization rate of cumulus-intact oocytes using *Slc35g3*^{+/-} and *Slc35g3*^{-/-}-derived sperm. Wilcoxon rank-sum test $P = 0.014$. (B) Outline of the procedure of cumulus cell-free IVF. (C) *Slc35g3*^{+/-}-derived and *Slc35g3*^{-/-}-derived sperm binding to cumulus-free oocytes after insemination. Scale bar = 50 μ m. (D) The number of bound sperm per egg for *Slc35g3*^{+/-}-derived and *Slc35g3*^{-/-}-derived sperm (Wilcoxon rank-sum test $P = 2.20 \times 10^{-18}$). (E) The fertilization rate of cumulus cell-free IVF using *Slc35g3*^{+/-}-derived and *Slc35g3*^{-/-}-derived sperm. (F) The procedure of ZP-free IVF. Wilcoxon rank-sum test; $P = 0.0079$. (G) Brightfield and Hoechst33342 staining of oocytes and

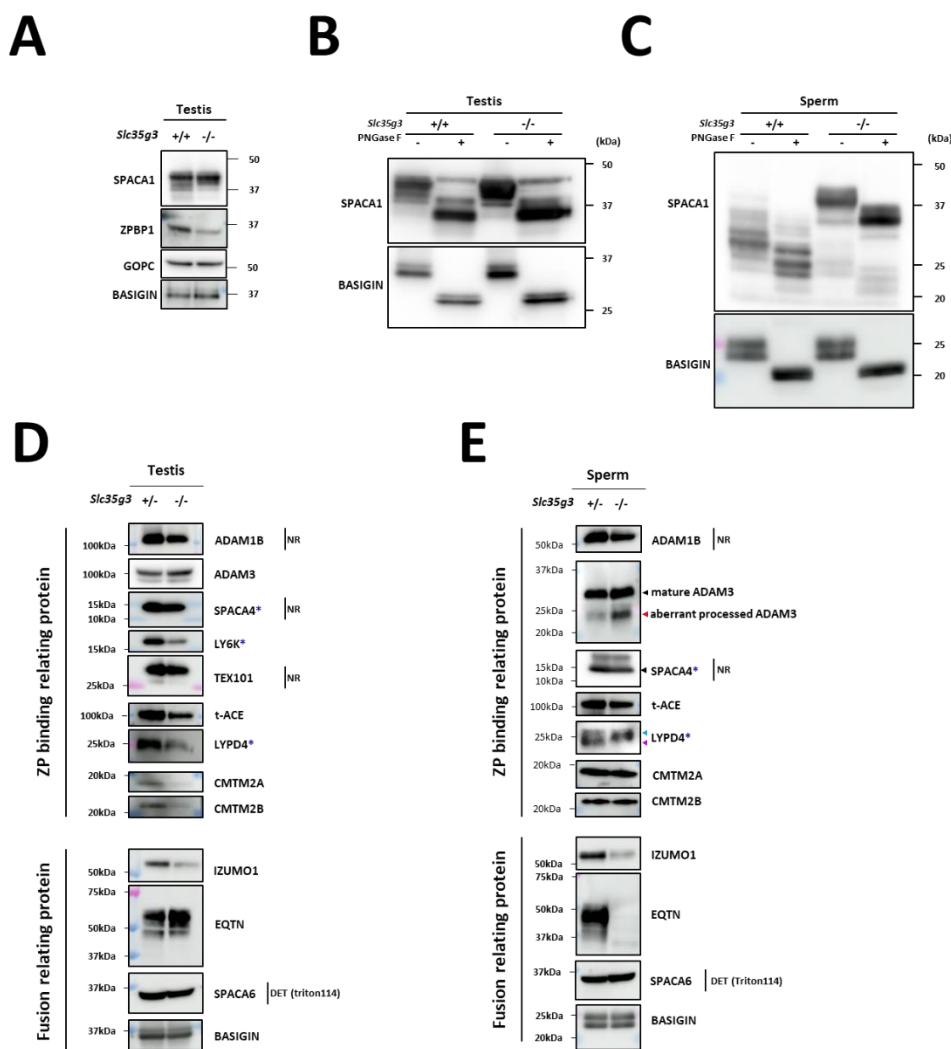
899 *Slc35g3*^{+/-}-derived and *Slc35g3*^{-/-}-derived sperm after insemination into ZP-free oocytes;
900 Yellow arrowheads indicate fused spermatozoa and light blue asterisks indicate
901 metaphase II-arrested chromosomes. (H) The number of fused sperm per egg using
902 *Slc35g3*^{+/-}-derived and *Slc35g3*^{-/-}-derived sperm (2×10^5 sperm/mL and 2×10^6 sperm/mL,
903 respectively). Significant differences are indicated by distinct symbols. (I) The
904 fertilization rate of ZP-free IVF using *Slc35g3*^{+/-}-derived and *Slc35g3*^{-/-}-derived sperm (2
905 $\times 10^5$ sperm/mL and 2×10^6 sperm/mL, respectively). Significant differences are
906 indicated by distinct symbols.

907



908

909 **Fig. 5. *Slc35g3*-deficient mice show impaired sperm migration to the oviduct**
910 (A) Illustration of Tg (CAG/su9-DsRed2, Acr3-eGFP) sperm. (B) A schematic diagram
911 of the sperm migration assay. (C) Bright field (top panel) and Dsred2 (bottom panel)
912 images of the uteri and oviducts of females after mating with control *Slc35g3*^{+/-} and
913 *Slc35g3*^{-/-} male mice. The yellow dashed line indicates the uterotubal junction (UTJ), and
914 the yellow arrowhead represents the sperm from control *Slc35g3*^{+/-} male mice that have
915 traversed the UTJ.
916



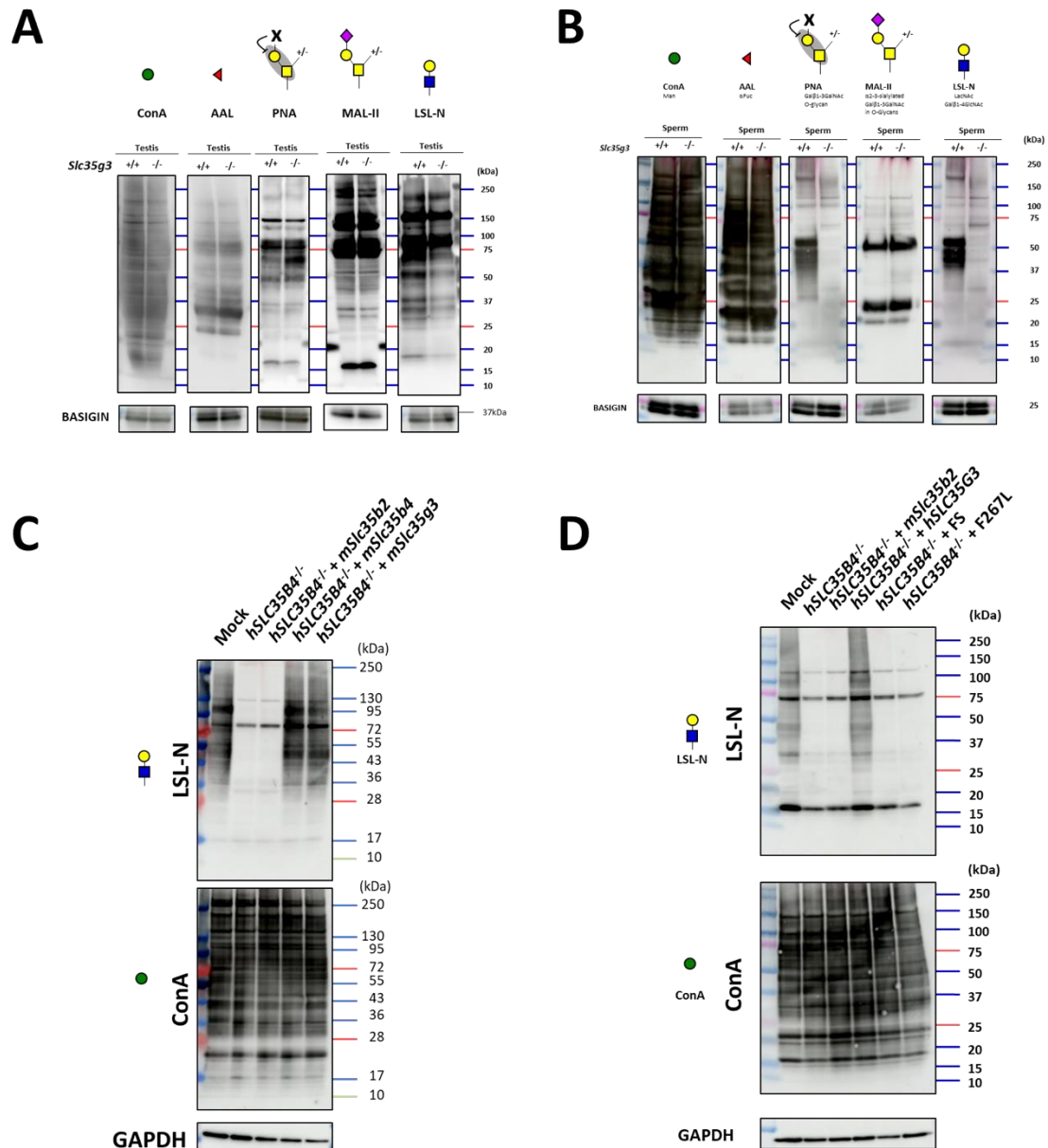
917

918 **Fig. 6. Disruption of *Slc35g3* leads to its reduced testicular expression and abnormal**
 919 **processing of multiple sperm proteins**

920 (A) Western blot analyses of SPACA1, ZPBP1, and GOPC in *Slc35g3*^{+/+} and *Slc35g3*^{-/-}
 921 testes, with BASIGIN used as a loading control. (B) Western blot analysis of PNGaseF
 922 treated or non-treated SPACA1 in *Slc35g3*^{+/+} and *Slc35g3*^{-/-} testes, with BASIGIN used as
 923 a loading control. (C) Western blot analysis of PNGaseF treated or non-treated SPACA1
 924 in *Slc35g3*^{+/+}-derived and *Slc35g3*^{-/-}-derived spermatozoa, with BASIGIN used as a
 925 loading control. (D) Western blot analyses of ADAM1B, ADAM3, SPACA4, LY6K,
 926 TEX101, t-ACE, LYPD4, CMTM2A, CMTM2B, IZUMO1, EQTN, and SPACA6 in
 927 *Slc35g3*^{+/+} and *Slc35g3*^{-/-} testes, with BASIGIN used as a loading control. All protein
 928 samples were processed under reducing and denaturing conditions unless otherwise
 929 specified. Non-reducing and non-denaturing conditions are denoted as NR. For SPACA6
 930 detection, fractions of testis proteins from wild-type and knockout specimens, extracted
 931 using Triton X-114, were utilized (abbreviated as DET). Genes marked with blue
 932 asterisks show reduced ZP binding upon knockout, whereas ADAM3 remains unaffected.
 933 (E) Western blot analyses of ADAM1B, ADAM3, SPACA4, t-ACE, LYPD4, CMTM2A,

934 CMTM2B, IZUMO1, EQTN, and SPACA6 in *Slc35g3*^{+/-}-derived and *Slc35g3*^{-/-}-derived
 935 spermatozoa, BASIGIN used as a loading control. The black arrowhead indicates the
 936 predicted protein size, whereas the red arrowhead indicates an aberrantly processed
 937 protein isoform. Additionally, the light blue and purple arrowheads mark the two bands
 938 observed in the wild-type sample.

939



940
941

942 **Fig. 7. *Slc35g3*^{-/-} testis showed impaired glycan structure**
 943 (A) Lectin blot (LB) analyses using ConA, AAL, PNA, MAL-II, and LSL-N in *Slc35g3*^{+/-}
 944 and *Slc35g3*^{-/-} testes, BASIGIN as a loading control. Green circles represent mannose, red

945 triangles fucose, yellow squares GalNAc, yellow circles galactose, purple diamonds sialic
946 acid, and blue squares GlcNAc. **(B)** LB analyses using ConA, AAL, PNA, MAL-II, and
947 LSL-N in *Slc35g3^{+/+}* and *Slc35g3^{-/-}* derived spermatozoa. **(C)** LB analyses of LSL-N and
948 ConA in SLC35B4 deficient HEK293T cells, with GAPDH as a loading control.
949 mSlc35b2, mSlc35b4 and mSlc35g3 were expressed in SLC35B4 deficient cells. **(D)** LB
950 analyses of LSL-N and ConA in hSLC35G3 mutant transfected SLC35B4 deficient cells,
951 with GAPDH, were used as a loading control. FS: T179HfsTer27.
952

953
954